

## Seismic-afterslip characterization of the 2010 $M_W$ 8.8 Maule, Chile, earthquake based on moment tensor inversion

Hans Agurto,<sup>1</sup> Andreas Rietbrock,<sup>1</sup> Isabelle Ryder,<sup>1</sup> and Matthew Miller<sup>2</sup>

Received 10 August 2012; revised 9 September 2012; accepted 11 September 2012; published 17 October 2012.

[1] On February 27th 2010, a  $M_W$  8.8 earthquake struck the coast of south-central Chile, rupturing  $\sim 500$  km along the subduction interface. Here we estimate the amount of seismically-released afterslip (SRA) and the mechanisms underlying the distribution of aftershocks of this megathrust earthquake. We employ data from a temporary local network to perform regional moment tensor (RMT) inversions. Additionally, we relocate global centroid-moment-tensor (GCMT) solutions, assembling a unified catalog covering the time period from the mainshock to March 2012. We find that most (70%) of the aftershocks with  $M_W > 4$  correspond to thrust events occurring on the megathrust plane, in areas of moderate co-seismic slip between 0.15 and 0.7 fraction of the maximum slip ( $S_{\max}$ ). In particular, a concentration of aftershocks is observed between the main patches of co-seismic slip, where the highest values of SRA are observed (1.7 m). On the other hand, small events,  $M_W < 4$ , occur in the areas of largest co-seismic slip ( $>0.85 S_{\max}$ ), likely related to processes in the damage zone surrounding the megathrust plane. Our study provides insight into the mechanics of the seismic afterslip pattern of this large megathrust earthquake and a quantitative approach to the distribution of aftershocks relative to coseismic slip that can be used for similar studies in other tectonic settings. **Citation:** Agurto, H., A. Rietbrock, I. Ryder, and M. Miller (2012), Seismic-afterslip characterization of the 2010  $M_W$  8.8 Maule, Chile, earthquake based on moment tensor inversion, *Geophys. Res. Lett.*, 39, L20303, doi:10.1029/2012GL053434.

### 1. Introduction

[2] Subduction zones, in which vast interplate strain is generated by the subduction of an oceanic plate under another plate, are the areas where the world's largest earthquakes occur, often resulting in great human and economic losses (e.g., Chile 1960, 2010; Sumatra 2004; Japan 2011). The  $M_W$  8.8 2010 Chile megathrust earthquake, the sixth largest seismic event ever recorded, ruptured nearly 500 km along the interface between the down-going Nazca plate and the overriding South America plate. The earthquake was responsible for large economic costs and, in conjunction with the subsequent tsunami, killed more than 525 people ([http://www.](http://www.interior.gob.cl/filesapp/listado_fallecidos_desaparecidos_27Feb.pdf)

[interior.gob.cl/filesapp/listado\\_fallecidos\\_desaparecidos\\_27Feb.pdf](http://www.interior.gob.cl/filesapp/listado_fallecidos_desaparecidos_27Feb.pdf)).

[3] The segment that ruptured in 2010 was previously identified as a mature seismic gap [Campos *et al.*, 2002; Ruegg *et al.*, 2009] and coincides with the region affected by a major earthquake ( $M \sim 8.5$ ) described by Darwin in 1835 [Lomnitz, 2004]. Since the 1835 event, major megathrust earthquakes have occurred within the area of the 2010 event in 1906, 1928, 1960 and 1985 [Campos *et al.*, 2002; Bilek, 2010], only partially rupturing the Darwin seismic gap (Figure 1).

[4] Several co-seismic slip models for the 2010 rupture have been published to date [e.g., Lorito *et al.*, 2011; Vigny *et al.*, 2011; Moreno *et al.*, 2012, and references therein], showing as a first order feature two high-slip patches located roughly to the north and south of the epicentre. Published aftershock distributions [e.g., Lange *et al.*, 2012; Rietbrock *et al.*, 2012] show seismicity concentrated between 10–35 km depth on the interface and then a second group at 40–45 km depth. Increased outer-rise seismicity is observed at the northern part of the rupture, whilst crustal events occur in the Pichilemu area [Ryder *et al.*, 2012].

[5] Previous studies on aftershock distributions, mainly of strike-slip faults [e.g., Mendoza and Hartzell, 1988], show that most of the aftershocks occur outside or near the edges of the areas of large slip. For a limited data set of subduction zone earthquakes, Das and Henry [2003] did not find a correlation between regions of high or low slip and aftershock occurrence, but argued that regions of high slip have fewer and smaller aftershocks. For the 2010 Maule earthquake, Rietbrock *et al.* [2012] analyzed three months of aftershocks and concluded that aftershocks are located preferentially in regions of rapid transition from high to low slip. In a recent study based on the analysis of aftershock focal mechanisms of the 2011 Tohoku-Oki, Japan, earthquake, Asano *et al.* [2011] found that interplate aftershocks with thrust faulting do not occur within the area of large co-seismic slip, but instead were localized in the surrounding regions.

[6] Here we present aftershock focal mechanisms (FMs) and corresponding centroid depths based on full waveform regional moment tensor (RMT) inversions of the largest aftershocks recorded on the International Maule Aftershock Dataset (IMAD) network. We also relocated focal solutions from the global centroid-moment-tensor (GCMT) project by using mislocation vectors derived from local observations. In this way, we assemble a catalog of FMs covering the whole time period since the mainshock (2010 February 27) up to March 2012. Utilizing this comprehensive catalog we produce a model of seismically-released afterslip (SRA) and discuss its relationship with published co-seismic and post-seismic slip models. Finally, we investigate the relationship

<sup>1</sup>School of Environmental Sciences, University of Liverpool, Liverpool, UK.

<sup>2</sup>Departamento de Geofísica, Universidad de Concepción, Concepción, Chile.

Corresponding author: H. Agurto, School of Environmental Sciences, University of Liverpool, Jane Herdman Building, Liverpool L69 3GP, UK. ([h.agurto@liv.ac.uk](mailto:h.agurto@liv.ac.uk))

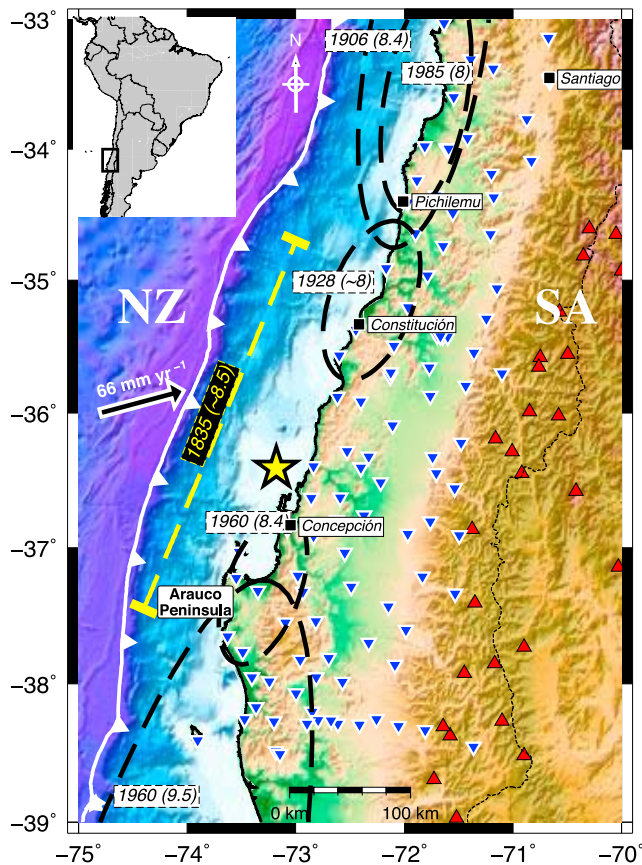


**Figure 1.** Location map. Yellow star indicates main shock [Vigny *et al.*, 2011]; inverted blue triangles show IMAD network and red triangles active volcanoes. Dashed black lines show approximate rupture areas of past megathrust earthquakes, including rupture extent of 1835 earthquake (dashed yellow line) [Campos *et al.*, 2002; Bilek, 2010]. NZ = Nazca Plate; SA = South America Plate. Topography/bathymetry GTOPO30.

of co-seismic slip and number of aftershocks using a quantitative approach.

[7] We aim to quantitatively describe the source characteristics and distribution of the 2010 aftershock sequence relative to the distribution of coseismic and postseismic slip, by employing a methodology that can be used to study any other subduction earthquake or, in general, any earthquake for which its sequence of aftershocks and a slip model are available.

## 2. Data and Methods

[8] We obtained RMT solutions for 125 earthquakes, from full waveform inversions, between March 18th and December 1st 2010. We employed data from the International Maule Aftershock Dataset (<http://www.iris.edu/mda/IMAD>; Figure 1) and used the software package ISOLA [Sokos and Zahradnik, 2008] to derive the RMT solutions. For each event we used its epicentral coordinates from an expanded version of the catalog of aftershocks published by Rietbrock *et al.* [2012], following their procedure. These authors used gap and number of observations criteria ( $\leq 270^\circ$  gap and more than 12 P-phase observations),

and a 2-D velocity model [Haberland *et al.*, 2009] to build their catalog of aftershocks. We then selected the bigger events ( $M > 4.5$ ) with a minimum of 20 P-phase observations (usually more than 60 P-wave observations) to invert for the RMT solutions.

[9] Additionally, we relocated 145 events from the GCMT catalog covering the aftershock sequence until March 2012. Earthquake relocations were calculated by averaging the differences in epicentral location for those events included in both the GCMT and our local catalog (Figure S1 in Text S1 in the auxiliary material).<sup>1</sup> The averaged mislocation vector (16 km in SE direction) is then used to relocate the GCMT events that occurred in absence of the local network.

[10] In order to calculate the amount of slip for each aftershock, we used the scaling relationships for subduction zones proposed by Blaser *et al.* [2010]. We obtained the associated slip by solving the equation for seismic moment [Aki, 1966], considering an average shear modulus  $\mu = 39$  GPa, which corresponds to an average S-wave velocity of 3.58 km/s [Haberland *et al.*, 2009] and a density of 3050 kg/m<sup>3</sup> [Tassara *et al.*, 2006] at megathrust seismogenic depths. Further details on methods and data processing are discussed in the auxiliary material.

## 3. Results and Discussion

[11] Thrust aftershocks occur mostly within  $\pm 5$  km depth of the subduction interface, except for those located north of the northern co-seismic slip patch, which are located at greater depth (Figures 2 and 3a). Notably, a high concentration of thrust events occurs north and south of the 8 m co-seismic slip contour of the northern co-seismic slip patch. P-axes of thrust interface events show a homogeneous distribution of azimuths concentrated in  $\sim$ E-W direction, orthogonal to the trench, with nearly all of them contained between  $260^\circ$  and  $290^\circ$  (Figure S3 in Text S1).

[12] The absence of major thrust aftershocks near the trench in front of the northern patch of co-seismic slip might indicate complete strain release during the mainshock's rupture, reaching shallow depths up-dip the megathrust as suggested by Vigny *et al.* [2011].

[13] Normal fault events tend to occur at shallower depths: (i) events in the Pichilemu area are located close to the coastline in the overriding plate at depths less than 20 km; (ii) increase of outer-rise seismicity occurs near the trench in front of the main co-seismic slip patch ( $34^\circ$ - $35^\circ$ S) and in front of the Arauco peninsula ( $\sim 37.6$  S) at shallow depths.

[14] Crustal normal-fault events in the Pichilemu area have been attributed to faulting induced by the Maule mainshock [Fariás *et al.*, 2011; Ryder *et al.*, 2012], in a similar setting to the crustal normal-fault seismicity described for the 2011 Tohoku-Oki earthquake by Kato *et al.* [2011]. Regarding the outer-rise normal fault events, it is widely accepted that outer-rise tensional events generally follow interplate ruptures in subduction zones, as demonstrated by Lay *et al.* [1989]. Slab bending and slab pull forces transmitted to the outer rise region due to the strain released by the mainshock can explain the increase in outer-rise seismicity observed in front of the northern and southern main slip patches.

<sup>1</sup>Auxiliary materials are available in the HTML. doi:10.1029/2012GL053434.

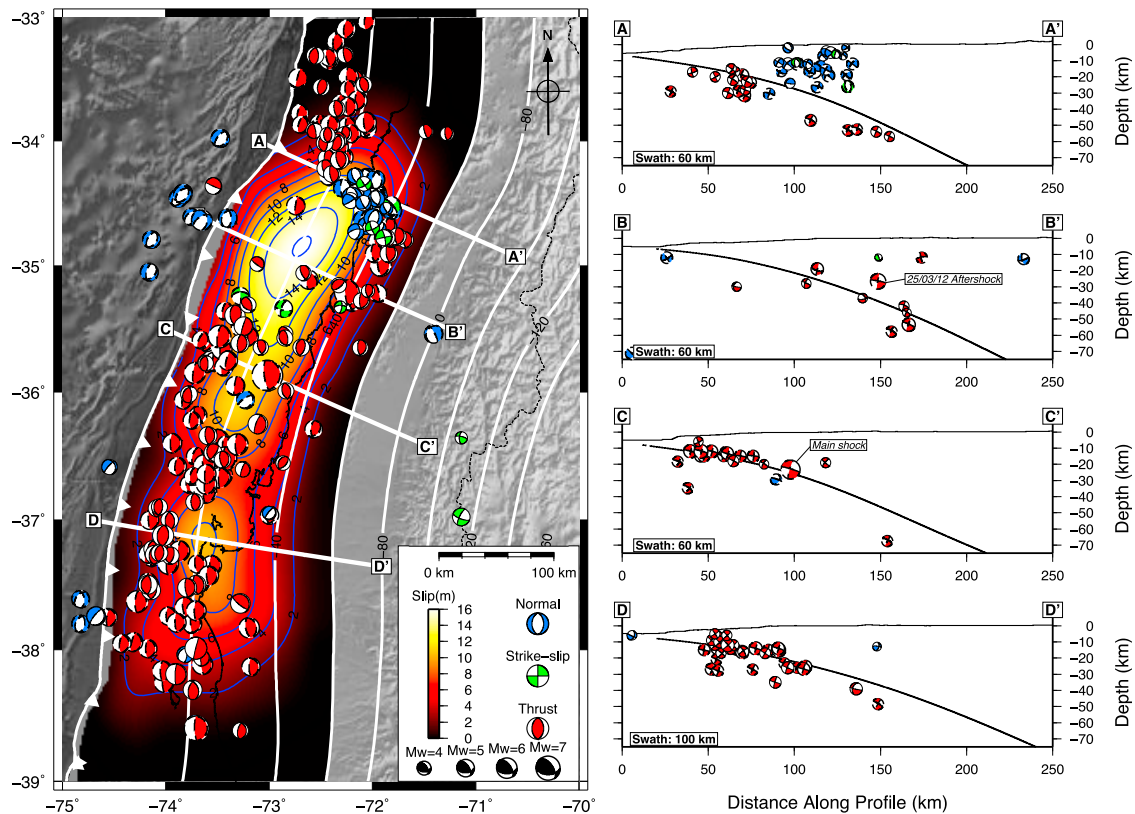


**Figure 2.** Distribution of FMs. (left) FMs are shown as lower half-sphere projection; color indicates fault type. FMs with solid outline are from this work; with dashed outline are relocated GCMT solutions. White contour lines show depth of the top of the slab [Hayes *et al.*, 2012]. Co-seismic slip model [Moreno *et al.*, 2012] is shown with blue contour lines every 2 m. White lines and uppercase letters indicate profiles shown in the right panel. (right) FMs are shown as far half-sphere projection on a vertical section. Solid thick black line indicates the top of the slab [Hayes *et al.*, 2012]; top black line shows topography/bathymetry.

[15] Strike-slip events are sparsely distributed in the overriding plate at shallow depths close to the coastline in the Pichilemu area and within the volcanic arc. Noteworthy is the strike-slip event  $M_w 5.1$  that occurred on 15th of August 2010, located at  $\sim 37^\circ\text{S}/71^\circ\text{W}$ , which corresponds to a NW left-lateral strike-slip fault associated with activity on the Nevados de Chillán volcano [Cembrano and Lara, 2009].

[16] Assuming that aftershocks occur in areas of rapid transition between high and low slip, surrounding high-slip regions of the mainshock [Rietbrock *et al.*, 2012], we compared our distribution of moment tensors with published co-seismic slip models. Our distribution of events correlates well with the key features of published slip models (Figure S4 in Text S1), although we favor the model proposed by Moreno *et al.* [2012] since we find an absence of aftershock thrust faulting within the two coseismic slip maxima (in particular in the northern patch, which presents the largest slip values) and aftershocks occurrence surrounding and delineating the zones of high co-seismic slip (Figures 2 and 3a). A similar distribution pattern has been reported for the aftershocks of the  $M_w = 9.0$  2011 Tohoku-Oki earthquake by Asano *et al.* [2011], and therefore might be characteristic of large megathrust earthquakes.

[17] Although aftershock studies of the 2010 Chile earthquake [e.g., Lange *et al.*, 2012; Rietbrock *et al.*, 2012] do show aftershock seismicity in the areas of high co-seismic

slip, this corresponds mostly to small ( $M < 4$ ) events, while there is a striking absence of major seismicity. All this indicates that most of the interplate stress was released during the mainshock, and therefore no major slip can occur postseismically on the main patches of co-seismic slip. On the other hand, stress introduced on dislocation tips in areas with high slip contrast, surrounding high-slip patches, will promote thrust faulting on the megathrust as observed in our data set (Figure 3a).

[18] Figure 3b shows the SRA model based on the cumulative seismic moment of thrust aftershocks located on the interface. The bulk of the afterslip (up to 1.7 m) is released offshore, between the two main patches of co-seismic slip at  $\sim 36.8^\circ\text{S}$ , followed by the afterslip due to the two largest aftershocks to date at  $38.7^\circ\text{S}$  ( $M_w 7.1$ ) and  $35.3^\circ\text{S}$  ( $M_w 7.2$ ), which occurred on the 2nd of January 2011 and 25th of March 2012, respectively. No afterslip is observed in the area of the two main co-seismic slip patches. Onshore, smaller afterslip is observed mainly in the Arauco peninsula and south of the Pichilemu area at  $\sim 35^\circ\text{S}$ .

[19] To our knowledge, the only afterslip model published to date is that of Vigny *et al.* [2011] based on GPS measurements for 12 days of postseismic deformation. In order to compare this afterslip with ours, we calculated the SRA for the first 12 days of postseismic activity (Figure 3c). Although the model by Vigny *et al.* [2011] shows two prominent patches of afterslip occurring onshore at  $\sim 35.7$

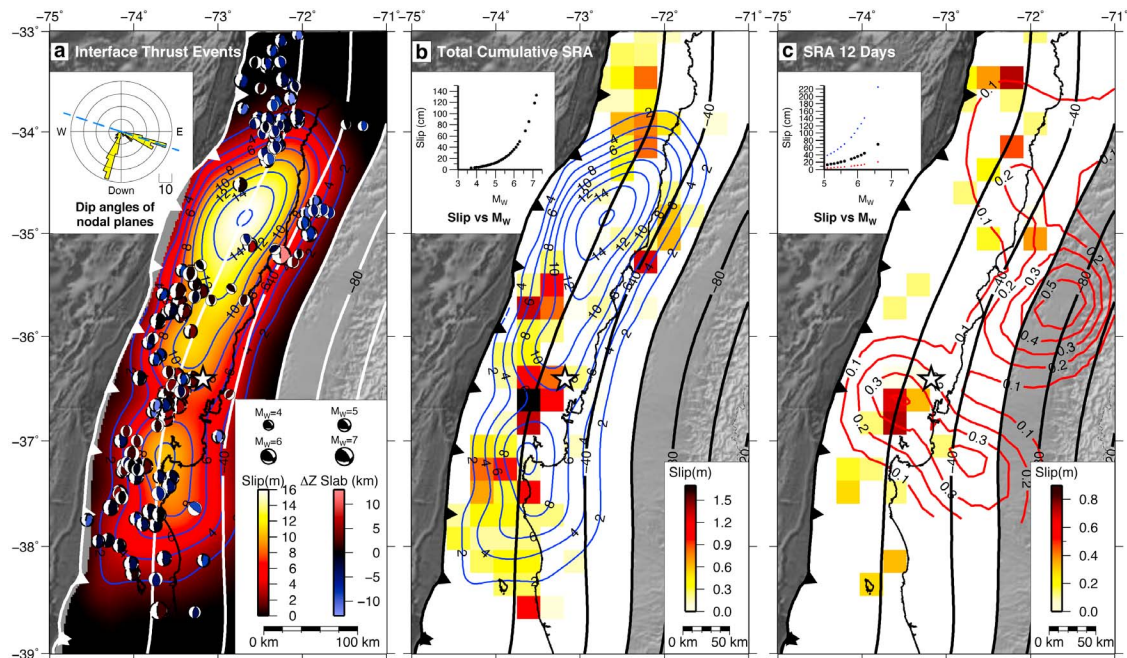


**Figure 3.** Interface thrust events and SRA model. Interface events were defined as those located at depths within 13 km (GCMT) and 6 km (this work) from the top of the slab respectively. Other features same as Figure 2. (a) Coseismic slip model [Moreno et al., 2012] and interface thrust events colored by vertical distance from the top of the slab. Inset: histogram of frequency of thrust events according to their nodal planes' dip angles; dashed blue line indicates dip angle of mainshock (megathrust plane). (b) Cumulative SRA. Inset: exponential relationship between calculated  $M_W$  and slip. (c) Cumulative SRA model for the 12-day period following the mainshock. Red contour lines show the 12-day postseismic afterslip model proposed by Vigny et al. [2011] every 0.1 m. Inset: same as 3b, including  $1\sigma$  of slip from scaling relationships (blue and red dots).

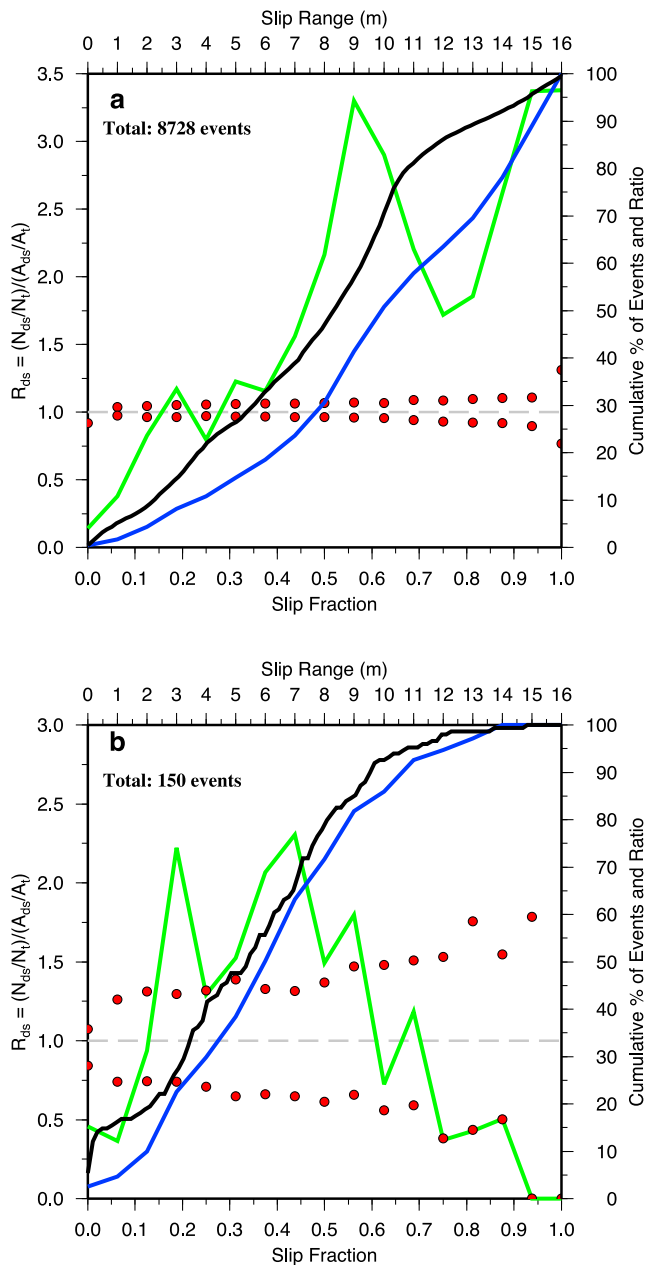


**Figure 4.** Histograms of aftershock distribution for (a) interface events from expanded catalog published by *Rietbrock et al.* [2012], (b) largest interface thrust events (as shown in Figure 3a). Green line shows  $R_{ds}$  values (left axis), blue line corresponds to the cumulative percentage of  $R_{ds}$  values (right axis), black line is the cumulative percentage of events (right axis). Red dots indicate one standard deviation values of  $R_{ds}$  for randomly distributed events test (see auxiliary material).

and  $\sim 37.2^{\circ}\text{S}$ , we do not observe such features, which indicates that the geodetically-measured afterslip might occur aseismically along deeper parts of the subduction interface. Offshore, both models show general agreement in the distribution of afterslip, in particular in the area between the two main patches of co-seismic slip ( $36^{\circ}$ – $37^{\circ}\text{S}$ ). However, for the significant afterslip patch at  $\sim 73.7^{\circ}\text{W}/36.8^{\circ}\text{S}$ , the SRA of 0.7 m is larger than the 0.4 m of afterslip inferred from geodetic observations. This discrepancy might be caused by

uncertainties in the scaling relationships (Figure 3c, inset) or the applied smoothing in the geodetic slip inversion.

[20] It is important to highlight the release of most of the seismic afterslip by several aftershocks with  $M_W < 6.8$  (cumulative equivalent  $M_W = 6.92$ ) in between the two main patches of co-seismic slip ( $\sim 36.8^{\circ}\text{S}$ ; Figures 3a and 3b), as opposed to the possible occurrence of an event  $M_W 7.5$ – $8.0$  in this area suggested by *Lorito et al.* [2011]. The afterslip in this zone is a persistent feature observed throughout the whole first year of postseismic activity.

[21] In order to quantify the correlation between the spatial patterns of aftershock locations and the distribution of co-seismic slip, we normalized the seismicity occurring in a given range of slip (e.g., 4–5 m) relative to the areal density of aftershocks for this slip range using a quantitative approach [*Hauksson, 2011*]. Thus, we define the ratio  $R_{ds} = (N_{ds}/N_t)/(A_{ds}/A_t)$ , where  $N_{ds}$  is the number of aftershocks occurring within a given range  $ds$  of slip,  $N_t$  is the total number of aftershocks,  $A_{ds}$  is the corresponding area covered by the range  $ds$  of slip, and  $A_t$  is the total area covered by the co-seismic slip (i.e., the area covered by the 0 m slip contour line). If  $R_{ds} > 1$ , the seismicity rate is considered to be greater than average rate, while if  $R_{ds} < 1$ , the seismicity rate is smaller than the average rate. The utilization of an areal normalization takes into account the inhomogeneous areal distribution of co-seismic slip models, as opposed to simply quantifying the cumulative distribution of aftershocks relative to co-seismic slip [e.g., *Woessner et al., 2006*].

[22] Figure 4a shows the obtained  $R_{ds}$  values for aftershocks located at interface depths (within 10 and 15 km above and below the top of the slab respectively) from the full catalog of aftershocks published by *Rietbrock et al.* [2012] as a fraction  $S$  of maximum slip. We observe that most of the aftershocks occur in areas with slip  $S > 0.3$ . A high rate of aftershocks in the fractional slip range  $0.4 < S < 0.75$  is observed and another peak is seen for areas with high slip ( $S > 0.85$ ). On the other hand, the normalized distribution of large interface thrust aftershocks (Figure 4b) shows that nearly 80% of these events occur in areas of moderate slip  $0.15 < S < 0.7$  (i.e., slip between 2 and 11 m) rather than in areas of high and low slip.

[23] Our results show that the largest ( $M_W > 4$ ) thrust aftershocks occur along the megathrust plane in areas of intermediate fractional slip ( $\sim 0.2$ – $0.7$ ), around patches of largest slip, accommodating stress increases resulting from the earthquake rupture process. Taking into account the whole magnitude range of aftershocks, a slightly different picture emerges. Smaller magnitude aftershocks ( $M < 4$ ) occur predominantly in areas of larger co-seismic slip, and are more loosely distributed laterally and in depth. Consequently, they might be associated with processes in the damage zone surrounding the megathrust plate interface, and could be triggered by coseismically-released fluids [e.g., *Nippress and Rietbrock, 2007*].

#### 4. Conclusion

[24] We determined RMT solutions from regional seismograms based on a full waveform inversion technique. Additionally, we re-located GCMT solutions leading to a combined catalog of 270 aftershock events. Thrust faulting dominates the postseismic seismicity, with also increased normal faulting in the outer-rise and Pichilemu area. SRA values obtained from

scaling relations indicate up to 1.7 m of afterslip at  $\sim 36.8^\circ\text{S}$  in the area between the two main co-seismic slip patches. Most of the SRA is observed offshore, with only marginal values observed inland.

[25] The distribution of the largest thrust aftershock events suggests that they occur at intermediate ranges of fractional co-seismic slip between 0.15–0.7. Small aftershocks are located in areas of high co-seismic slip ( $>0.85 S_{\text{max}}$ ) and are likely linked to processes in the damage zone surrounding the megathrust plane (e.g., fluids release and re-activation of pre-existent secondary structures).

[26] The present catalog of moment tensor solutions, derived SRA model, and histograms of aftershock distribution can be used as a reference for future afterslip studies, providing constraints on the spatio-temporal aftershock distribution of the 2010 Chile megathrust earthquake. Our comparison of SRA and published geodetic afterslip models provides insight into the mechanisms underlying the occurrence of afterslip recorded by geodetic/seismic networks. Moreover, our study offers a quantitative measure of the distribution of aftershocks relative to coseismic slip that can be applied to other large subduction earthquakes.

[27] **Acknowledgments.** HA thanks J. Zahradnik and E. Sokos for their support in the usage of ISOLA; and CONICYT, Chile, through its program of scholarships ‘Beca Presidente de la República’. We received funding from NERC (NE/I005420/1). Seismic instruments were provided by CNRS-INSU, IRIS/PASSCAL, GIPP(GFZ), GEF/SeisUK (Loan 922). Figures were done with software GMT [Wessel and Smith, 1998].

[28] The Editor thanks one anonymous reviewer for assisting in the evaluation of this paper.

## References

- Aki, K. (1966), 4. Generation and propagation of G waves from the Niigata earthquake of June 14, 1964. Part 2. Estimation of earthquake moment, released energy and stress strain drop from G wave spectrum, *Bull. Earthquake Res. Inst. Univ. Tokyo*, 44, 73–88.
- Asano, Y., T. Saito, Y. Ito, K. Shiomi, H. Hirose, T. Matsumoto, S. Aoi, S. Hori, and S. Sekiguchi (2011), Spatial distribution and focal mechanisms of aftershocks of the 2011 off the Pacific coast of Tohoku earthquake, *Earth Planets Space*, 63(7), 669–673, doi:10.5047/eps.2011.06.016.
- Bilek, S. (2010), Invited review paper: Seismicity along the South American subduction zone: Review of large earthquakes, tsunamis, and subduction zone complexity, *Tectonophysics*, 495, 2–14, doi:10.1016/j.tecto.2009.02.037.
- Blaser, L., F. Kruger, M. Ohmberger, and F. Scherbaum (2010), Scaling relations of earthquake source parameter estimates with special focus on subduction environment, *Bull. Seismol. Soc. Am.*, 100(6), 2914–2926, doi:10.1785/0120100111.
- Campos, J., et al. (2002), A seismological study of the 1835 seismic gap in south-central Chile, *Phys. Earth Planet. Inter.*, 132(1–3), 177–195, doi:10.1016/S0031-9201(02)00051-1.
- Cembrano, J., and L. Lara (2009), The link between volcanism and tectonics in the southern volcanic zone of the Chilean Andes: A review, *Tectonophysics*, 471(1–2), 96–113, doi:10.1016/j.tecto.2009.02.038.
- Das, S., and C. Henry (2003), Spatial relation between main earthquake slip and its aftershock distribution, *Rev. Geophys.*, 41(3), 1013, doi:10.1029/2002RG000119.
- Fariás, M., D. Comte, S. Roecker, D. Carrizo, and M. Pardo (2011), Crustal extensional faulting triggered by the 2010 Chilean earthquake: The Pichilemu seismic sequence, *Tectonics*, 30, TC6010, doi:10.1029/2011TC002888.
- Haberland, C., A. Rietbrock, D. Lange, K. Bataille, and T. Dahm (2009), Structure of the seismogenic zone of the south-central Chilean margin revealed by local earthquake travel-time tomography, *J. Geophys. Res.*, 114, B01317, doi:10.1029/2008JB005802.
- Hauksson, E. (2011), Crustal geophysics and seismicity in Southern California, *Geophys. J. Int.*, 186, 82–98, doi:10.1111/j.1365-246X.2011.05042.x.
- Hayes, G., D. Wald, and R. Johnson (2012), Slab1.0: A three-dimensional model of global subduction zone geometries, *J. Geophys. Res.*, 117, B01302, doi:10.1029/2011JB008524.
- Kato, A., S. Sakai, and K. Obara (2011), A normal-faulting seismic sequence triggered by the 2011 off the Pacific coast of Tohoku earthquake: Wholesale stress regime changes in the upper plate, *Earth Planets Space*, 63(7), 745, doi:10.5047/eps.2011.06.014.
- Lange, D., et al. (2012), Aftershock seismicity of the 27 February 2010  $M_w$  8.8 Maule earthquake rupture zone, *Earth Planet. Sci. Lett.*, 317–318, 413–425, doi:10.1016/j.epsl.2011.11.034.
- Lay, T., L. Astiz, H. Kanamori, and D. Christensen (1989), Temporal variation of large intraplate earthquakes in coupled subduction zones, *Phys. Earth Planet. Inter.*, 54(3–4), 258–312, doi:10.1016/0031-9201(89)90247-1.
- Lomnitz, C. (2004), Major earthquakes of Chile: A historical survey, 1535–1960, *Seismol. Res. Lett.*, 75(3), 368–378, doi:10.1785/gssrl.75.3.368.
- Lorito, S., et al. (2011), Limited overlap between the seismic gap and coseismic slip of the great 2010 Chile earthquake, *Nat. Geosci.*, 4(3), 173–177, doi:10.1038/ngeo1073.
- Mendoza, C., and S. Hartzell (1988), Aftershock patterns and main shock faulting, *Bull. Seismol. Soc. Am.*, 78(4), 1438–1449.
- Moreno, M., et al. (2012), Toward understanding tectonic control on the  $M_w$  8.8 2010 Maule Chile earthquake, *Earth Planet. Sci. Lett.*, 321–322, 152–165, doi:10.1016/j.epsl.2012.01.006.
- Nippres, S. E. J., and A. Rietbrock (2007), Seismogenic zone high permeability in the Central Andes inferred from relocations of micro-earthquakes, *Earth Planet. Sci. Lett.*, 263(3–4), 235–245, doi:10.1016/j.epsl.2007.08.032.
- Rietbrock, A., I. Ryder, G. Hayes, C. Haberland, D. Comte, S. Roecker, and H. Lyon-Caen (2012), Aftershock seismicity of the 2010 Maule  $M_w$  = 8.8, Chile, earthquake: Correlation between co-seismic slip models and aftershock distribution?, *Geophys. Res. Lett.*, 39, L08310, doi:10.1029/2012GL051308.
- Ruegg, J., A. Rudloff, C. Vigny, R. Madariaga, J. D. Chabaliere, J. Campos, E. Kausel, S. Barrientos, and D. Dimitrov (2009), Interseismic strain accumulation measured by GPS in the seismic gap between Constitución and Concepción in Chile, *Phys. Earth Planet. Inter.*, 175(1–2), 78–85, doi:10.1016/j.pepi.2008.02.015.
- Ryder, I., A. Rietbrock, K. Kelson, R. Bürgmann, M. Floyd, A. Socquet, C. Vigny, and D. Carrizo (2012), Large extensional aftershocks in the continental forearc triggered by the 2010 Maule earthquake, Chile, *Geophys. J. Int.*, 188, 879–890, doi:10.1111/j.1365-246X.2011.05321.x.
- Sokos, E., and J. Zahradnik (2008), ISOLA a Fortran code and a MATLAB GUI to perform multiple-point source inversion of seismic data, *Comput. Geosci.*, 34(8), 967–977, doi:10.1016/j.cageo.2007.07.005.
- Tassara, A., H. Gotze, S. Schmidt, and R. Hackney (2006), Three-dimensional density model of the Nazca plate and the Andean continental margin, *J. Geophys. Res.*, 111, B09404, doi:10.1029/2005JB003976.
- Vigny, C., et al. (2011), The 2010  $m_w$  8.8 Maule megathrust earthquake of central Chile, monitored by GPS, *Science*, 332(6036), 1417–1421, doi:10.1126/science.1204132.
- Wessel, P., and W. Smith (1998), New, improved version of generic mapping tools released, *Eos Trans. AGU*, 79(47), 579, doi:10.1029/98EO00426.
- Woessner, J., D. Schorlemmer, S. Wiemer, and P. Mai (2006), Spatial correlation of aftershock locations and on-fault main shock properties, *J. Geophys. Res.*, 111, B08301, doi:10.1029/2005JB003961.